JOURNAL OF CATALYSIS 63, 476–486 (1980)

Morphology of Supported Metal Clusters: Determination by EXAFS and Chemisorption

R. B. GREEGOR AND F. W. LYTLE

The Boeing Company, Seattle, Washington 98124

Received August 6, 1979; revised February 5, 1980

When small metal clusters are examined by EXAFS the apparent average coordination number is smaller than that observed in the bulk metal because of the high proportion of surface atoms. This effect is dependent on the size and shape of the metal cluster. Geometrical shape models have been derived for spheres, cubes, and disks which give the EXAFS average coordination number for first, second, and third coordination spheres as a function of cluster size. Dispersion models (via chemisorption measurements) are also presented for different cluster shapes and sizes. For a correct choice of shape these two types of observations should predict the same cluster size. Results for the models are presented with experimental data for a variety of supported catalysts. Electron microscopy is used to support the analyses where possible.

INTRODUCTION

Supported metal catalysts are known to differ remarkably in catalytic activity due to differences in preparation or conditioning. Changes in metal particle size, size distribution, and shape may be important variables. Information concerning the size and shape of supported metal clusters can be obtained by several techniques (*1*) including high-resolution electron microscopy (*2*), X-ray diffraction (*3*), chemisorption (*4*), and, as reported here, extended X-ray absorption fine structure (EXAFS). EXAFS is a technique of X-ray spectroscopy in which the ejected photoelectron acts as a probe of the surrounding environment in a manner similar to electron scattering. Since the absorption edges of different elements are well separated in energy the technique is element specific and able to examine the surroundings of a specific catalytic element in the presence of the support.

In this paper we develop particle shape models as a function of particle size and show that the sensitive variable, average coordination number, as determined by EXAFS, can be used to examine size and shape. Then in concert with chemisorption data and dispersion models we find an indication of particle size and shape for some supported catalysts. Electron microscopy data are used to support the analysis where possible.

GEOMETRICAL SHAPE MODELS

In order to establish limiting trends for models of shape and size, we have chosen the following extreme examples of geometrical shapes: spheres, cubes, and disks. In all our models we have assumed face-centered-cubic (fcc) packing. Similar analyses have been reported previously (*5*). Depending on relative height to diameter, disks can represent the total range of shapes from an extended monolayer raft, to cylinders, to extended rod-like particles. The model of a thin disk deserves special consideration in that there is electron microscopy evidence (*2*) for some supported catalysts in which disk-like aggregates are found which appear to be quite thin and for which the dispersion approaches unity. A one- or two-layer disk appears to be the best shape to explain these data.

Calculation of Average Coordination Number

As shown in Fig. 1a, a two-region model was used to determine the average coordi-

0021-9517/80/060476-11$02.00/0

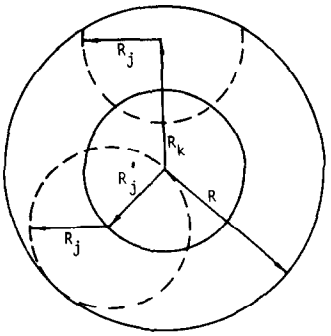

a) SPHERES

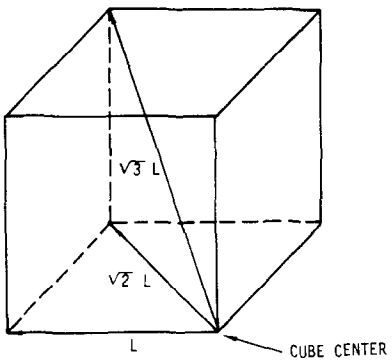

b) CUBES

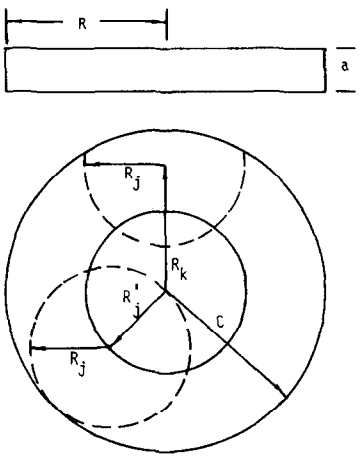

c) DISCS

FIG. 1. Shape models depicting the various regions used in determining the average coordination number for (a) spheres, (b) cubes, and (c) disks.

nation number for spherical particles. The inner region denoted by R_j' was defined so that any atom within R_j' had a coordination sphere R_j which was unterminated by the spherical particle boundary at R. These radii are related by $R_j' = R - R_j$, where the values of j are 1, 2, or 3 corresponding to the first, second, and third coordination sphere. Atoms located in the outer region R_k (defined by $R_j' < R_k \leq R$) had coordination spheres terminated by the particulate boundary. The fraction F of a given coordination sphere in the outer region which laid within the particle was given by

$$F = \tfrac{1}{2}\left[1 + \frac{R^2 - R_k^2 - R_j^2}{2R_kR_j}\right]$$

where

$$R_k = k^{1/2}a.$$

The shortest interatomic distance was a and the value of k was an integer representing the coordination sphere count beginning with the atom at the center of the particles. The outer-region atoms reduced the effective average coordination number for the ensemble of atoms within the particulate boundary. For a given coordination sphere with coordination N_j (R_j and N_j were determined by the crystal structure; see Table 1) the average coordination number $\bar{N}_j$ was calculated using a formula involving an expression for both regions as follows:

TABLE 1

Parameters for Assumed fcc Structure[a]

$j = R_j^2/a^2$	R_j (Å)	N_j	n_j
1	2.75	12	6
2	3.89	6	0
3	4.75	24	6
4	5.50	12	6

[a] a is the shortest interatomic distance; j designates the first, second, etc., coordination sphere; R_j is the radius of the coordination sphere, $R_1 = a = 2.75$ Å was used as an average value for the size/shape figures; N_j is the number of atoms in each coordination sphere; n_j is the number of atoms in each coordination sphere in a monolayer parallel to the (111) plane.

$$\bar{N}_j = \frac{1}{R^3}\left[(R - R_j)^3 N_j + \sum_k (3\Delta R_k^2 + 3\Delta^2 R_k + \Delta^3) F N_j\right].$$

The first expression within brackets is proportional to the product of N_j and the number of atoms within the inner region. The second expression is a summation over successive coordination shells of radius R_k in the outer region. The summation of k was performed so that $(R - R_j) < R_k \leq R$. Each of the terms in the summation was proportional to the product of the number of atoms in the R_kth shell and the number of atoms in terminated coordination spheres at distance R_j away from an atom in the R_kth shell. The average coordination number is the sum of the expressions for both regions divided by R^3, which is proportional to the total number of atoms within the particle radius. For a packing fraction of 0.75, corresponding to the fcc structure, the radius was related to the total number of atoms N_T within the particle by

$$R = \frac{a}{1.82}(N_T)^{1/3},$$

where a is the shortest interatomic distance. The shell increment Δ is the difference between R_k and R_{k+n}. The value of n determines the size of the increment used in the summation. Usually for $N_T < 1000$, $n = 1$ and for larger particles $n > 1$ was used.

A cuboidal particle can also be divided into an inner unterminated region and outer regions. Again the inner region was constructed so that any atom inside its boundary had a coordination sphere which was unterminated by the particle boundary. For the cubic case the k shells in the outer regions as well as the j coordination spheres were terminated by the particulate boundary. Three shell factors F_s were required depending on the value of R_k as shown in Fig. 1b. For $R_k \leq L$, $F_s = 1$. For the two outer regions F_s was similar to F of the spherical case. The coordination factor F_c depended on the location of $R_k - R_j$ and $R_k + R_j$ in the region diagram of Fig. 1b. The possible combinations give rise to nine regional coordination factors of the form of F. The shell factors F_s were applied to coordination spheres which were constructed about an atom in the center of the particle while the coordination factors F_c were applied to coordination spheres centered on atoms in the outer two regions. The average coordination number was given by a sum of expressions for the inner and outer regions:

$$\bar{N}_j = \frac{\pi}{6L^3}\left[(L - R_j)^3 N_j + \sum_k F_s(3\Delta R_k^2 + 3\Delta^2 R_k + \Delta^3) F_c N_j\right].$$

The cube half-side L was related to the total number of atoms in the particle by

$$L = \frac{a}{2.25}(N_T)^{1/3}.$$

The expressions for R_k, R_j, N_j, and Δ were the same as for the spherical case. The summation in k was performed so that $(L - R_j) < R_k \leq 3^{1/2}L$.

The two-region model shown in Fig. 1c was sufficient for the case of a monolayer disk. We have chosen an orientation in which the (111) plane was parallel to the surface of the support as being most probable for fcc or hcp metals. The radius C of a disk of height a, packing in the (111) plane, was related to the total number of atoms N_T by

$$C = \frac{a}{2.12}(N_T)^{1/2}.$$

The average coordination number for such a monolayer disk was given by

$$\bar{N}_j = \frac{1}{C_2}\left[(C - R_j)^2 N_j + \sum_k (2\Delta R_k + \Delta^2) F_d n_j\right].$$

Here n_j was the coordination number when all atoms resided in a single plane (see Table 1). The values of R_k, R_j, N_j, and Δ were as given previously. F_d was the fraction of n_j residing within the particulate boundary and was given by an expression

similar to F. The summation in k was performed so that $(C - R_j) < R_k \leq C$. Multiple-layer disks also were constructed using arguments similar to those given above.

The ratio of $\bar{N}_j/N_j$ as a function of the total number of atoms N_T in the particle for the three cases studied is shown in Fig. 2. In each case the first few coordination spheres were considered and are indicated by $j = 1, 2, 3$, or 4. For large particles ($N_T > 100$) the majority of atoms reside within the inner regions and $\bar{N}_j \cong N_j$ so that the ratio $\bar{N}_j/N_j$ asymptotically approaches 1 for spheres and cubes at large values of N_T. For monolayer disks at large values of N_T the first coordination sphere does not asymptotically approach a value of 1 because not all of the atoms in this coordination sphere reside in the (111) plane. Since only six atoms of the first coordination sphere reside in the (111) plane the ratio $\bar{N}_1/N_1$ asymptotically approaches a value of 0.5. Also note that for this case the second coordination sphere is absent because these atoms are above and below the (111) plane.

For the case of a hypothetical catalyst with metal particles of a unique size and shape we would expect separate experimental measurements of $\bar{N}_j/N_j$ for the first, second, and third coordination spheres to predict the same particle size, within experimental error, on the correct shape model graph. As will be apparent in the data, this is often not the case. In particular, if there exists a distribution of shapes which in-

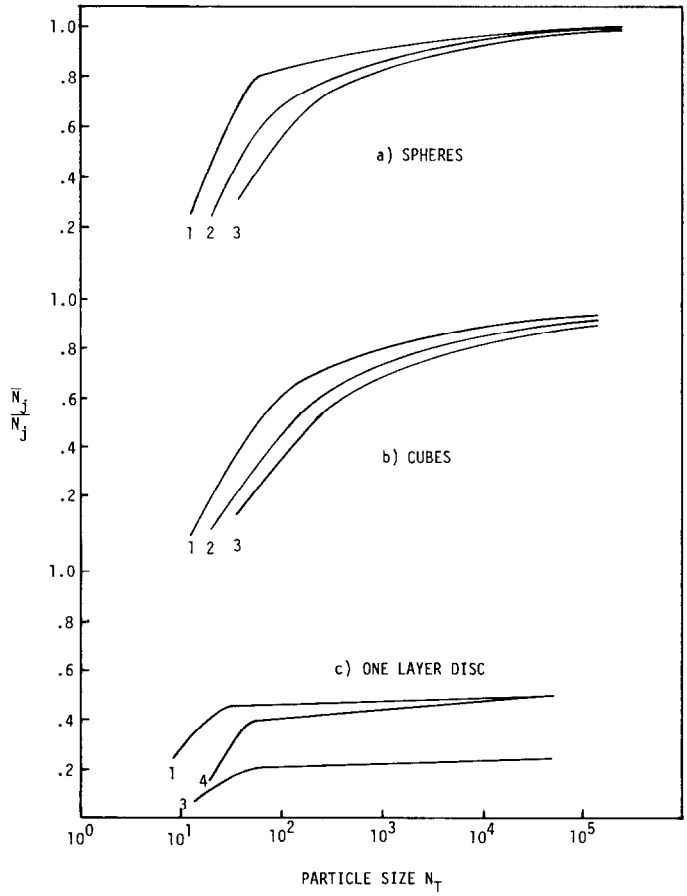

FIG. 2. The ratio of $\bar{N}_j/N_j$ ($j = 1, 2, 3, 4$) as a function of the total number of atoms N_T in the particle for (a) spheres, (b) cubes, and (c) disks.

cludes monolayer (111) oriented disks the $\bar{N}_2/N_2$ will predict significantly lower particle sizes than $\bar{N}_1/N_1$ or $\bar{N}_3/N_3$. This occurs because the second coordination sphere is completely absent from the monolayer disk as was discussed previously.

Dispersion Models

The dispersion D of a supported metal catalyst is defined as the surface fraction of metal atoms. In the limiting case where every surface atom absorbs one gas atom the dispersion is just equal to the surface to volume ratio for a given particle shape and size. However, the active sites may not always be comprised of only one surface atom. For these cases analytical expressions for the number of surface atoms having various sets of incomplete nearest-neighbor shells can be derived (*6*).

The surface to volume ratio for spheres, cubes, and disks is plotted as a function of size in Figs. 3a and 3b. The same surface to volume curve can be used for spheres and cubes if the abscissas used are the sphere radius R and cube half-side L (see Figs. 1a and 1b). For R equal to L there are more surface atoms for the cubes but the number of bulk atoms is also larger, thus keeping the surface to volume ratio constant. Obviously, for one- or two-layer disks, the surface to volume ratio is independent of particle size since all the atoms are surface atoms. For three or more layers the surface/volume ratio is dependent on particle size. Also it can be seen that surface/volume ratios lying to the right of the dotted line in Fig. 3b indicate structures which are disk-like (height $\ll$ diameter) and those lying to the left are rod-like (height $\gg$ diameter).

For all models of shape and size for a supported catalyst there is an open question as to the availability for chemisorption

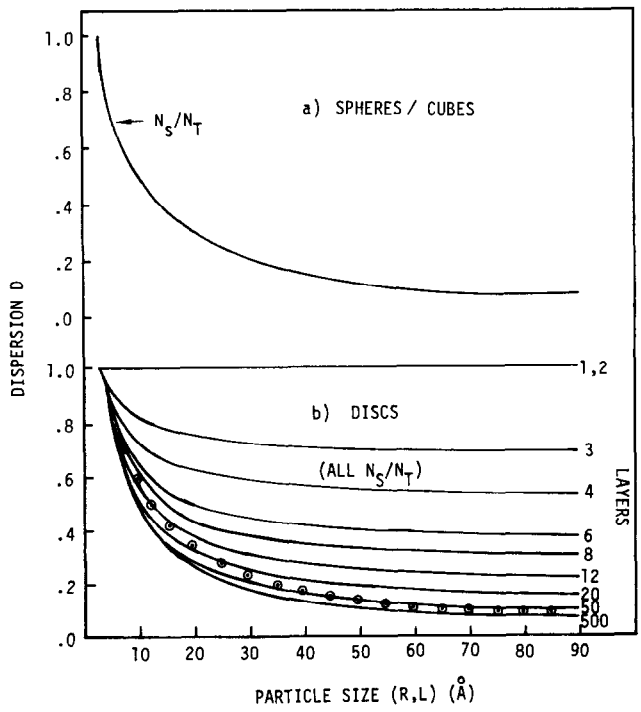

FIG. 3. The dispersion D (assuming an interatomic distance of 2.75 Å) as a function of particle size for (a) spheres/cubes and (b) disks. The dotted line in (b) represents the demarcation between disk-like (height $\ll$ diameter) and rod-like (height $\gg$ diameter) structures. N_s refers to the number of surface atoms and N_T the total number of atoms in the particle.

of the side of the metal particles in contact with the support, i.e., is there complete or only slight blocking of chemisorbing atoms? We know of no conclusive data regarding this question; however, there are indications of fairly large raft-like or disk-like particles in catalysts where the dispersion measured by chemisorption approaches unity. If these are thicker than a single layer, then both sides of the particle must be mostly available for chemisorption. Consequently, we have used the full surface area for all particle shapes considered and allowed no support effect. Reducing the surface area of each shape by the estimated area in contact with the support (which is probably not the full geometrical area) would not materially affect our results and could be included within the estimated uncertainty.

DATA AND ANALYSIS

All of the EXAFS data were obtained at the Stanford Synchrotron Radiation Laboratory, on the EXAFS I spectrometer (*7*). The temperature of measurement of both the reference metals and the catalysts was 100 ± 5 K. The catalyst preparation and treatment has been described (*8, 9*). All were examined in the reduced condition under a hydrogen atmosphere. Except for the 0.63 wt% Cu on SiO_2 catalyst the EXAFS data and analysis have been previously reported for 1 wt% Ru on SiO_2 (*8*) and 1 wt% Os, Ir, and Pt on SiO_2 and 1 wt% Ir and Pt on Al_2O_3 (*9*). These data and results will be used in the present analysis of size and shape. An example of the EXAFS data, Fourier transform, and the fitted data for the first coordination shell is given in Fig. 4. Shown in Fig. 5 are the Fourier transforms for selected reference metals and catalysts. In addition to the 1st shell coordination numbers reported previously we have evaluated the second and third shell coordination numbers for a few cases. This was done by comparing fitted parameters for data from each pure-metal reference and the respective catalyst. The data were Fourier-filtered to isolate just the contribution of the second and third coordination shells. This function was then fit to determine coordination number by using calculated forms of the EXAFS phase shift (*10*) and backscattering amplitude (*11*). From the coordination number for each metal and catalyst the ratios $\bar{N}_j/N_j$ ($\bar{N}_j$ denotes the catalyst and N_j the metal coordination number) were calculated as given in Table 2.

Comparison was made to known reference compounds in order to estimate the accuracy of determination of $N_1 = \pm 20\%$ (*8*). As yet this has not been possible for N_2 and N_3. We expect the error to be somewhat larger than for N_1. Therefore, no error limits are noted for N_2 and N_3 in Table 2 or on the plots of $\bar{N}/N_j$ vs size in Fig. 6. $\bar{N}_1/N_1$ for the first coordination shell were relatively high for Ru, Cu, and Ir and lower for Os and Pt. The lower values allow the possibility of thin disk-like shapes. In general, for a given catalyst $\bar{N}_j/N_j$ decreased with increasing coordination shell.

The dispersion data of Table 2 have been extracted from Refs. (*8*) and (*9*) and are primarily from room-temperature CO chemisorption, i.e., a system most likely to result in 1 : 1 stoichiometry of one CO molecule per metal surface atom.

SIZE AND SHAPE DETERMINATION

The average coordination number and dispersion can be used to investigate the sizes and shapes of small catalytic particles. Some insight can be gained regarding the nature of the active sites of the catalysts by requiring agreement between sizes predicted by the two types of models for a given shape. Agreement between the two models was determined by first plotting the ratio $\bar{N}_j/N_j$ on a graph of the ratio of the average coordination number for each shape as shown by the examples in Fig. 6. The abscissa has been modified using the known interatomic distance to show particle size. The uncertainty in $\bar{N}_1/N_1$ of each data point (±20%) is indicated. Next, tak-

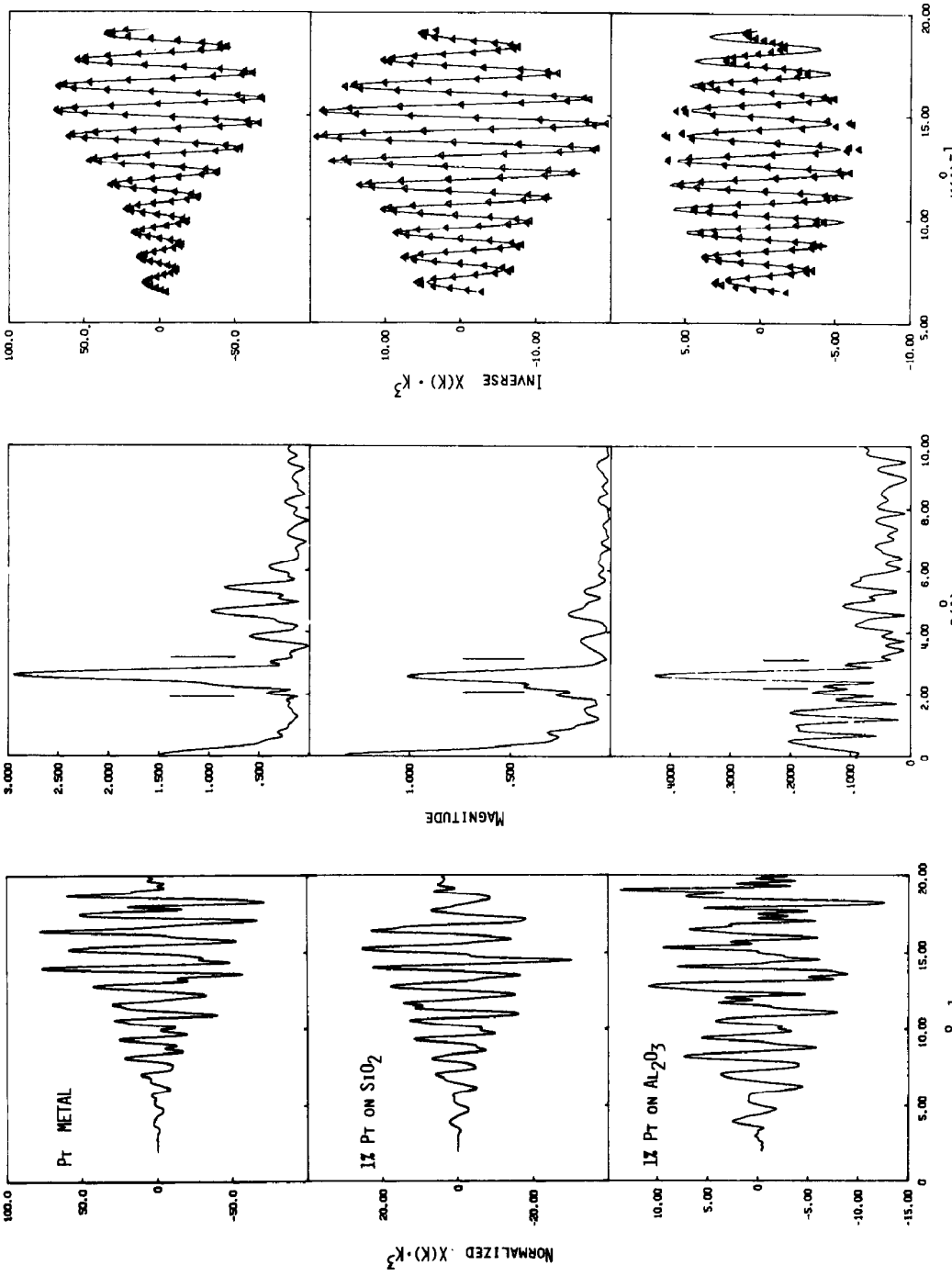

FIG. 4. An example of EXAFS data $\chi(k)\cdot k^3$ vs k, the Fourier transform magnitude, and first shell inverse transforms for Pt metal and catalysts (at 100 K). The range of the inverse transform is indicated by the vertical lines on either side of the first shell peak. The inverse transform is the solid line, the plotted points indicate the least-squares fit.

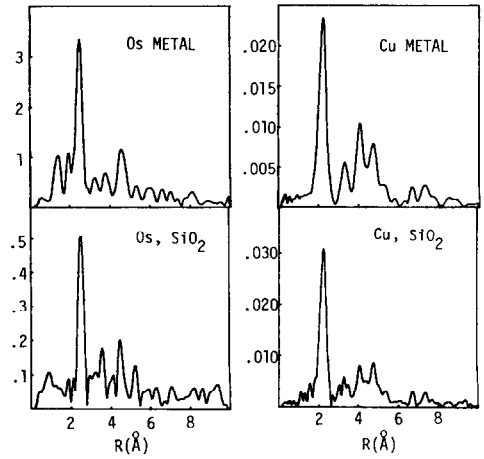

FIG. 5. Fourier transforms of the bulk metal and catalysts of Os and Cu. All at 100 K, transform range from 3–20 Å^{-1}, k^3 transforms from Os, k^1 transforms for Cu.

ing the measured dispersion of the catalyst given in Table 2, the set of graphs relating particle size and dispersion (Fig. 3) was used to predict a size for each shape. This size (the vertical line in Fig. 6) and its estimated error (shaded) were plotted on the same graph as the $\bar{N}_j/N_j$. (Note that there is no dispersion size information possible for one- or two-layer disks since for this shape the surface to volume ratio = 1 and is independent of size.) For each catalyst examined we sought the one shape with the best agreement, within the two regions of uncertainty, between the size estimated by $\bar{N}_j/N_j$ and that estimated from dispersion. For a correct shape these two methods of measurement should predict the same particle size. This was the primary criterion used for establishing the shape tendencies listed in Table 3. The first coordination shell was the major consideration in the size and shape analysis because the errors in N_2 and N_3 were uncertain. Also, note that in all cases each surface atom was identified as a reaction site (the curves N_S/N_T in Fig. 3a,b). Presumably, this would not be the case for reactions with more complex molecules. For some catalysts a clear choice of shape trend was evident and for others no clear-cut choice was possible, perhaps indicating a distribution of shapes. In all cases there was quite good agreement of the size estimates by the EXAFS and dispersion techniques for the indicated shape tendency. The average of the two size indications (average coordination and dispersion) is listed in Table 3.

As discussed above and shown by the $\bar{N}_j/N_j$ plot of Fig. 2C, the second coordination sphere is completely missing for a monolayer disk and diminished proportionately for "thin" disks of a few layers' thickness. This feature is a useful diagnostic for the presence of thin disk-like structures. The second peak of the Fourier transform was present in all cases indicating that in none of the catalysts do monolayer disks predominate; however, the Pt on Al_2O_3 catalyst shown in Fig. 4 has a diminished or shifted second peak suggesting the possibility of a significant population of thin disk-like structures. Further-

TABLE 2

Summary of EXAFS and Chemisorption Results

Catalyst	1st shell $\bar{N}_1/N_1$	2nd shell $\bar{N}_2/N_2$	3rd shell $\bar{N}_3/N_3$	Dispersion	Molecule
Os on SiO_2	0.68 ± 20%	0.33	—	1.0 ± 20%	CO
Ru on SiO_2	0.92	0.70	—	0.5	CO
Cu on SiO_2	0.92	0.73	—	0.3	O
Pt on SiO_2	0.67	0.26	0.56	0.7	H
Pt on Al_2O_3	0.60	—	—	0.9	H, CO, O
Ir on SiO_2	0.83	0.28	0.26	0.8	CO
Ir on Al_2O_3	0.83	0.33	0.21	0.9	CO, O

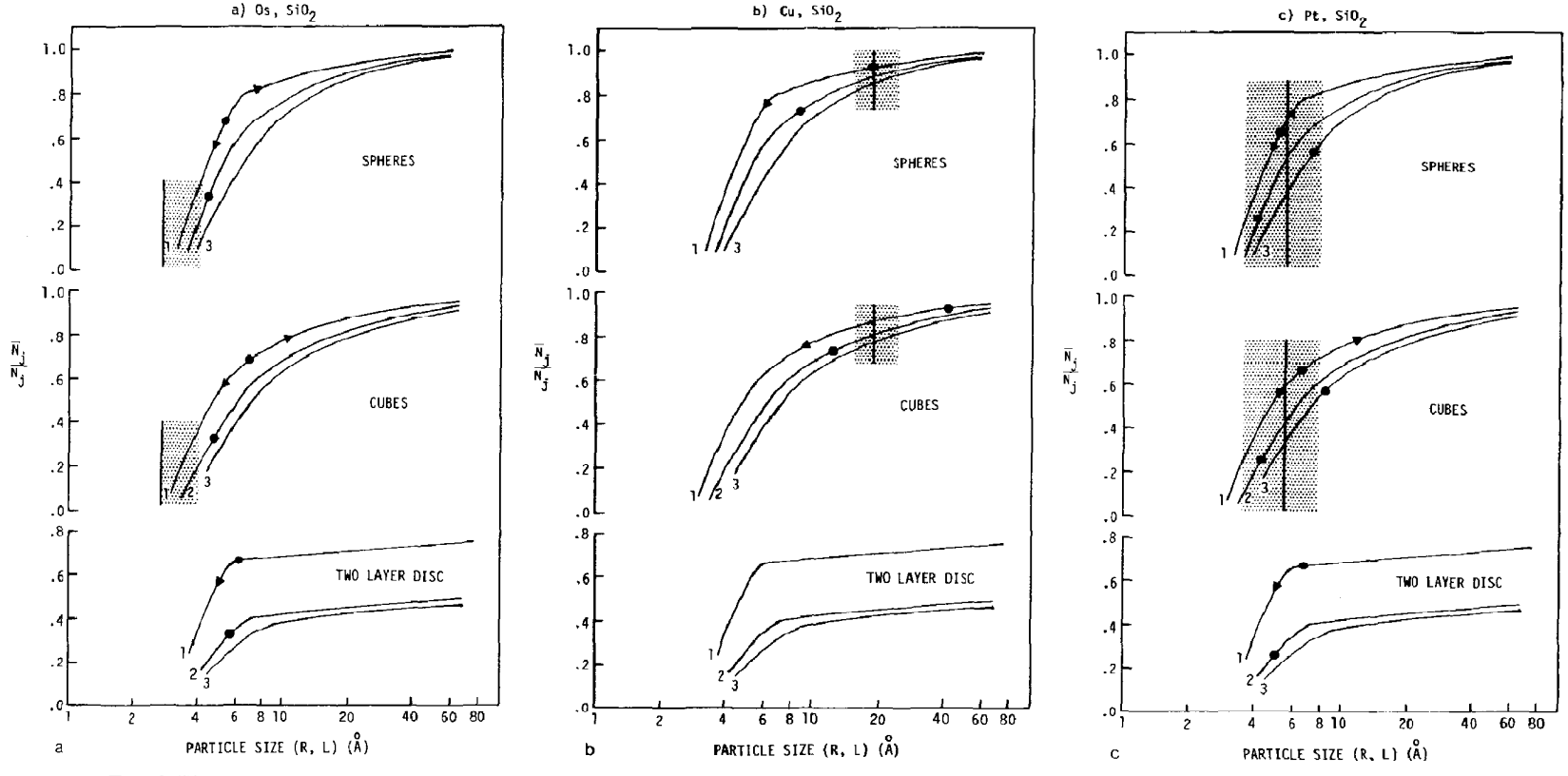

FIG. 6. The particle sizes predicted by dispersion (vertical line with ±20% error shading) and average coordination number (data points with ±20% errors) superimposed on the plots of average coordination number vs particle size. That shape resulting in the best agreement between the two methods of measurement was selected as the shape trend. Note that for a two-layer disk no dispersion size information is possible, i.e., $D = 1$. Error bars are not known for second and third coordination spheres. The +20% error bars ran off the graph for the first coordination sphere of some cases and is therefore not shown. (a) For Os the data could not be fit to the sphere or cube models, therefore the disk-like shape seemed most probable. Note at ~2.75 Å only the +20% error is shown for the dispersion data since smaller sizes are not possible. (b) Best agreement for Cu was for sphere-like shapes. (c) All shapes seem equally possible on the basis of this analysis for the Pt catalysts. This suggests a distribution of shapes.

TABLE 3

Summary of Size and Shape Tendencies

Catalyst	Radius of metal particle (Å)		
	Disk (minihedra)	Cubes (midihedra)	Spheres (maxihedra)
Os on SiO_2	7 ± 2 (6)[a]		
Ru on SiO_2			14 ± 7 (18)[a]
Cu on SiO_2			19 ± 5
Pt on SiO_2[b]	7 ± 3	6 ± 2	5 ± 2
Pt on Al_2O_3[b]	5 ± 2	5 ± 2	4 ± 3
Ir on SiO_2			6 ± 2
Ir on Al_2O_3			6 ± 3

[a] Value in parentheses indicates weighted average size taken from electron microscopy of Prestridge *et al.* (*2*).

[b] Shape trend uncertain and may indicate distribution of shapes.

more, there is a general trend of low $\bar{N}_2/N_2$ in some of the size/shape graphs indicating a relatively smaller size than the first shell, which suggests that in all of these catalysts there are present monolayer disk-like shapes. If our data were sufficiently accurate we could estimate the relative proportions of a shape mix, but for now simply note the trend.

The Cu and Ru catalysts both appear to be primarily spherical. Electron microscopy (*2*) indicated that for Ru there was a distribution of small disks and larger spheres with a weighted average radius of 18 Å. This is apparently consistent with the present result of 14-Å spheres in that most of the atoms are contained within the larger spherical particles. Both Ir catalysts can be assigned spherical shapes although as noted before, the $\bar{N}_2/N_2$ is low which may indicate a significant contribution due to thin disks. The Pt catalysts cannot be assigned to a unique shape, i.e., all shapes investigated appear equally possible. This may be evidence of a real distribution of shapes. The Pt on Al_2O_3 has a diminished and shifted second coordination shell which may indicate a substantial population of thin disk-like shapes. The Os catalyst had the highest dispersion (1.0) of the catalysts studied here and exhibited a disk-like shape tendency. The size result, radius equal to 7 Å, is close to the electron microscopy measurement of 6 Å which also found a preponderance of disk-like shapes having a narrow size distribution (*2*).

DISCUSSION

This work has demonstrated the feasibility of measuring size and shape of small metal particles using the EXAFS technique. The determinable parameter is the average coordination number which is related to particle size and shape calculations. Shape information is included since the average coordination number is sensitive to shape. The average coordination number is most sensitive in the region below 20 Å,, which is the region inaccessible or difficult by X-ray diffraction or electron microscopy. There is no lower size limit on making EXAFS measurements; indeed, accuracy improves for very small metal clusters of a few atoms (*9*). However, for clusters of a few atoms the average coordination number is not a good discriminator of shape. As used here, shape agreement was sought for size estimates based upon both EXAFS and chemisorption data. Coincidence in size established the shape trend; however, a good estimate of size alone for cubes or spheres could be made from either data since shape is a second-order effect for these shapes. EXAFS used alone can establish the presence of thin disks because of certain limits in $\bar{N}_j/N_j$ and the absence of 2nd coordination spheres which is inherent in close packing of metal atoms. Improvements in data gathering and data processing may allow eventual estimates of both size and shape distributions within the necessary constraints of the model calculations from EXAFS data alone.

Where comparison was possible there was good agreement between this size estimate and that previously done by electron microscopy on portions of the same catalyst preparation. However, there is a serious caveat in such comparisons because the EXAFS results were on clean catalysts reduced *in situ* and the microscopy (as well

as X-ray diffraction results (*3*)) were obtained on air-exposed catalysts. Our EXAFS work in progress has shown that the structure of many supported metal catalysts is significantly altered by atmospheric exposure.

Finally the assumption of specific shapes in the model calculations should not be viewed as absolute. We emphasize this in Table 3 by noting the general categories associated with the three shapes investigated. Minihedra refer to shapes having two sides, disks or rafts. Midihedra are shapes having approximately six sides more or less equal in area, e.g., cubes. Maxihedra are those shapes having many sides where a sphere can be considered as a reasonable approximation to the shape.

ACKNOWLEDGMENTS

We thank G. Via and J. Sinfelt, Exxon for chemisorption data on the Cu catalyst and for helpful discussions. We are grateful to Stanford Synchrotron Radiation Laboratory which is funded by NSF for the experimental time. Our research was funded by NSF Grants CHE 76-11255 and DMR 77-12919.

REFERENCES

1. Whyte, T. E., Jr., *Catal. Rev.* **8**(1), 117 (1973).
2. Prestridge, E. B., Via, G. H., and Sinfelt, J. H., *J. Catal.* **50**, 115 (1977).
3. Sashital, S. R., Cohen, J. B., Burwell, R. L., Jr., and Butt, J. B., *J. Catal.* **50**, 479 (1977).
4. Sinfelt, J. H., *Progr. Solid State Chem.* **10**, 55 (1975); *Science* **195**, 641 (1977).
5. a) Greegor, R., and Lytle, F., Paper presented at Stanford Synchrotron Radiation Laboratory Users Group Meeting, Stanford University, 1977. b) Cook, J., Sayers, D., and Brown, M., Paper presented at Stanford Synchrotron Radiation Laboratory Users Group Meeting, Stanford University, 1978.
6. Van Hardeveld, R., and Artog, F. H., *Surface Sci.* **15**, 189 (1969).
7. Eisenberger, P., Kincaid, B., Hunter, S., Sayers, D., Stern, E., and Lytle, F., "Proc. IV Int. Conf. on Vac. U.V. Rad. Phys. Hamburg, July 22–26," p. 806, 1974.
8. Lytle, F., Via, G., and Sinfelt, J., *J. Chem. Phys.* **67**, 3831 (1977).
9. Via, G. H., Sinfelt, J. H., and Lytle, F. W., *J. Chem. Phys.* **71**, 690 (1979).
10. Lee, P. A., Teo, B. K., and Simons, A. L., *J. Amer. Chem. Soc.* **99**(11), 3856 (1977).
11. Teo, B. K., and Lee, P. A., *J. Amer. Chem. Soc.* **191**(11), 2815 (1979).